Supersonic thermal excitation-induced shock wave in black phosphorene

Jige Chen,[1,*] Shunda Chen,[2] and Yi Gao[1]

[1]*Division of Interfacial Water and Key Laboratory of Interfacial Physics and Technology, Shanghai Institute of Applied Physics, Chinese Academy of Sciences, Shanghai 201800, China*

[2]*Department of Chemistry, University of California Davis, Davis, California 95616, USA*

(Received 5 December 2016; published 4 April 2017)

Thermal transport in low-dimensional materials possesses various novel features since anomalous energy carriers may heavily contribute. Black phosphorene exhibits excellent thermal properties and thus it attracts attention about the possible existence of anomalous energy carriers. In this paper, we find that shockwave appears as a dominant energy carrier in the zigzag direction of black phosphorene when a supersonic thermal excitation above a critical strength is exerted. Comparing with the diffusive thermal transport, shockwave carries a considerable amount of excitation energy and propagates faster than the local acoustic speed. It leads to a strong anisotropic enhancement in the transport speed of thermal energy in the zigzag direction, up to a factor of twofold compared with no shockwave. The linear increase of velocity with intensity and exponential decay of intensity with time of the shockwave are observed. Unlike solitary waves, the collision of shockwaves exhibits no phase shift in the spatial-temporal trajectory. Moreover, it shows that shockwave velocity decreases with tensile strain, which is favorable for modulation. Our results reveal a possible anomalous energy transport process and may help in designing black phosphorene-based thermal devices.

DOI: 10.1103/PhysRevB.95.134301

I. INTRODUCTION

Recent years have witnessed enduring interest of thermal energy transport in low-dimensional materials due to the practical issue for heat removal and energy conversion in the electronics industry [1–21]. Comparing with bulk materials, low-dimensional materials exhibit various novel thermal features, where the collective motions due to nonlinearity other than phonons, referred to anomalous energy carriers [1,2,22–26], could heavily contribute. Theoretical studies of thermal conduction in two-dimensional (2D) and 1D nonlinear crystals have shown that anomalous energy carriers, such as effective phonons [22] and solitary waves [24–26], are conjectured to be related to the microscopic mechanism of exotic properties like thermal rectification [8,27–30] and thermal conductivity divergence [1,2,31,32]. Since the effect of nonlinearity comes with the relatively large interaction, an usual method to identify an anomalous energy carrier is to apply a strong supersonic heat pulse on the low-dimensional crystal, where the abrupt change in the medium could induce anomalous leading wave fronts [1,24–26,33–38].

Meanwhile, theoretical and experimental work has shown the evidence of anomalous energy carriers, i.e., supersonic and subsonic solitary waves, in 1D carbon nanotube [30,39,40] and 2D graphene [28,41,42]. It stimulates great interest in finding anomalous energy carriers in noncarbon low-dimensional materials. Black phosphorene (BP), a single layer of phosphorus atoms arranged in a stacked honeycomb lattice, has attracted growing attention as a new member in the 2D material family [14,43–48]. Recent experimental work shows that it possesses an excellent anisotropic thermal property that is preferentially along the zigzag direction than the armchair direction [5,6]. Our recent work further shows that thermal anisotropy is anomalously enhanced rather than suppressed when it is supported on a substrate [38]. Such novel thermal behavior implicates the possible existence of anomalous energy carriers.

In this paper, we study thermal energy transport of BP under supersonic thermal excitation by molecular dynamics simulations. Interestingly, it is found that shockwave appears as a dominant energy carrier exclusively in the zigzag direction when the excitation strength is above a critical value. Shockwave carries a considerable amount of energy away faster than the local acoustic speed, leading to a strong enhancement in the thermal energy transport speed. Furthermore, for utilizing shockwave in possible application, its kinetic behavior, e.g., the intensity, velocity, collision and strain modulation, are also investigated.

II. METHODS

The schematic of the system is shown in Fig. 1(a), in which the armchair or the zigzag edges of the BP sheet will be excited by a heat pulse. The dimension of the BP sheet is 300×300 Å^2 with the armchair direction along the x axis and the zigzag direction along the y axis. A fixed boundary condition is applied on the edge atoms in both axes to avoid overall translation and the edge effect could be neglected (please see PS2 in the Supplemental Material [49]). The interaction between the adjacent phosphorus atoms is described by the Stillinger-Weber (SW) potential with valence force field parametrization [50–52] which includes bond stretching, introgroup angle bending, intergroup bending, and multibody terms. The parameters could reproduce the phonon dispersion, negative Poisson' s ratio, and stress-induced bending in *ab initio* calculations [46,51] and are applied to calculate thermal conductivity [38,50,52] and fracture behavior [53] in molecular dynamics simulations. The results in this manuscript are also stable by modifying the SW parameters and further details are provided in PS3 in the Supplemental Material. An open-source package, LAMMPS [54], is used to perform all the simulations.

*chenjige@sinap.ac.cn

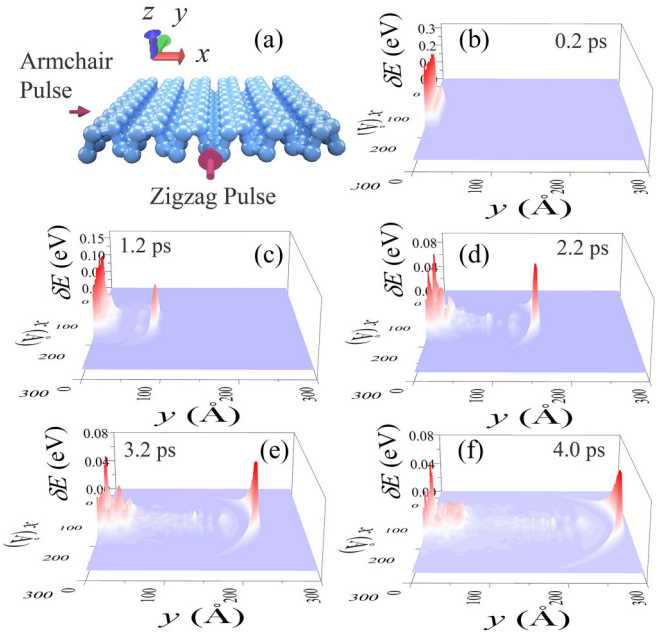

FIG. 1. (a) Schematic of thermal excitation in a BP sheet. BP (blue crystal) is placed with the armchair direction along the x axis and the zigzag direction along the y axis. A heat pulse (red arrow) generates thermal excitation on the middle 1/3 of the outermost atoms on the armchair edge (armchair pulse) or the zigzag edge (zigzag pulse) to initiate the respective thermal energy transport. [(b)–(f)] Thermal energy transport function, δE, as a function of x and y in the zigzag direction under excitation strength $\chi_S = 30$ at simulation time 0.2–4.0 ps. The leading wave profile, which leaves the fluctuating wave packets far behind, represents a shockwave induced by the zigzag pulse.

The simulations include the armchair and zigzag excitations by adding a heat pulse on the middle 1/3 of the outermost atoms (the fixed edges are excluded), which is a process similar to side excitation in our recent work [38]. First, an energy minimization is initially performed and the BP sheet is equilibrated at the ground state to diminish thermal fluctuations for 100 ps. Therefore, the exerted excitation would correspond to phonon response at the low-temperature limit. Then a heat pulse is added onto the armchair or the zigzag edges by adding the kinetic velocity $v_x = \chi_S$ km/s or $v_y = \chi_S$ km/s on the phosphorus atoms. Here χ_S denotes the excitation strength and when $\chi_S \geqslant 10$ (or $\chi_S \leqslant 5$) it refers to a supersonic (or subsonic, as a comparison) thermal excitation. The excitation method [1,24–26,33–38] provides an idealized scenario of thermal energy transport by tracing the propagation wave packets of the heat pulse.

III. RESULTS AND DISCUSSION

Figures 1(b)–1(f) illustrate the typical profile of shockwave in the zigzag direction induced by a supersonic thermal excitation with $\chi_S = 30$. It is characterized by the thermal energy transport function as [23,38]

$$\delta E(x,y,t) = E(x,y,t) - E_0(x,y,t), \quad (1)$$

where E represents the energy of each phosphorus atoms in the BP sheet with the exerted heat pulse and E_0 represents the energy of phosphorus atoms in the same BP sheet with exactly the same initial condition but excluding the heat pulse. The snapshots of δE provide the propagating profiles of the heat pulse. Meanwhile, to better illustrate the emergence of the shockwave and the associated critical value of excitation strength, the time variation of δE under different excitation strength, e.g., $\chi_S = 1$ and 5 (subsonic thermal excitation without shockwave generation), $\chi_S = 20$ (supersonic thermal excitation without shockwave generation), and $\chi_S = 25$ and 30 (supersonic thermal excitation with shockwave generation) are shown in Figs. 2(a)–2(d).

As shown in Fig. 2, in the subsonic zigzag excitation $\chi_S = 1$ and 5, a series of fluctuating wave packets are excited and propagate along the BP sheet, just like a ripple in a pond. When the interaction amplitude is comparatively small, the harmonic part of the interaction would play the dominant role in determining the excited-wave profile. Therefore, the excited-wave profiles under different χ_S values are almost identical subject to a proper rescaling. The quasi-identical fluctuating wave profiles correspond to the phonon response that acts as normal energy carriers in the BP sheet to the subsonic thermal excitations. Here the speed of the leading wave peak corresponds to the local acoustic speed in the zigzag direction and is denoted as V_a. Furthermore, the local acoustic speed exhibits strong anisotropy in the zigzag and armchair directions (please see PS1 in the Supplemental Material).

On the other hand, in the strong supersonic zigzag excitation $\chi_S = 25$ and 30, a single high leading wave front emerges and propagates faster than the local acoustic speed. The leading wave front represents the shockwave response to the supersonic thermal excitations. There are four noticeable features to distinguish the shockwave response from the phonon response as follows.

The first one is that there is a critical value of excitation strength $\chi_S = 25$ which is necessary for the shockwave generation. As shown in Fig. 2, below that critical value, even with a supersonic thermal excitation, for example, with $\chi_S = 20$, no shockwave could be excited and a similar phonon response to the subsonic excitation is observed. Such an excitation strength requirement is well known in the formation of a solitary wave in low-dimensional crystal. It represents the minimal nonlinearity requirement [55,56] since the formation of anomalous energy carriers relies on the nonlinear steepening of an ordinary wave and nonlinearity rises with interaction amplitude.

The second feature is that the shockwave propagates at a speed, denoted as V_s, higher than the local acoustic speed V_a [55,57,58]. It represents the nonlinear response to the abrupt supersonic change in the BP sheet and thus it is also dependent on the interaction amplitude. Later we show that V_s is linearly dependent on the shockwave intensity in Fig. 3(d). As a comparison, in the subsonic and supersonic excitation without shockwave generation, the wave fronts propagate at the same speed V_a.

The third feature is that the shockwave leaves a tail of turbulent sonic boom. As shown in Figs. 1(d)–1(f), the sharp-nosed wave peak moves with a left- and a right-running bowlike wave tails. The wave pattern [55,57,58] resembles the

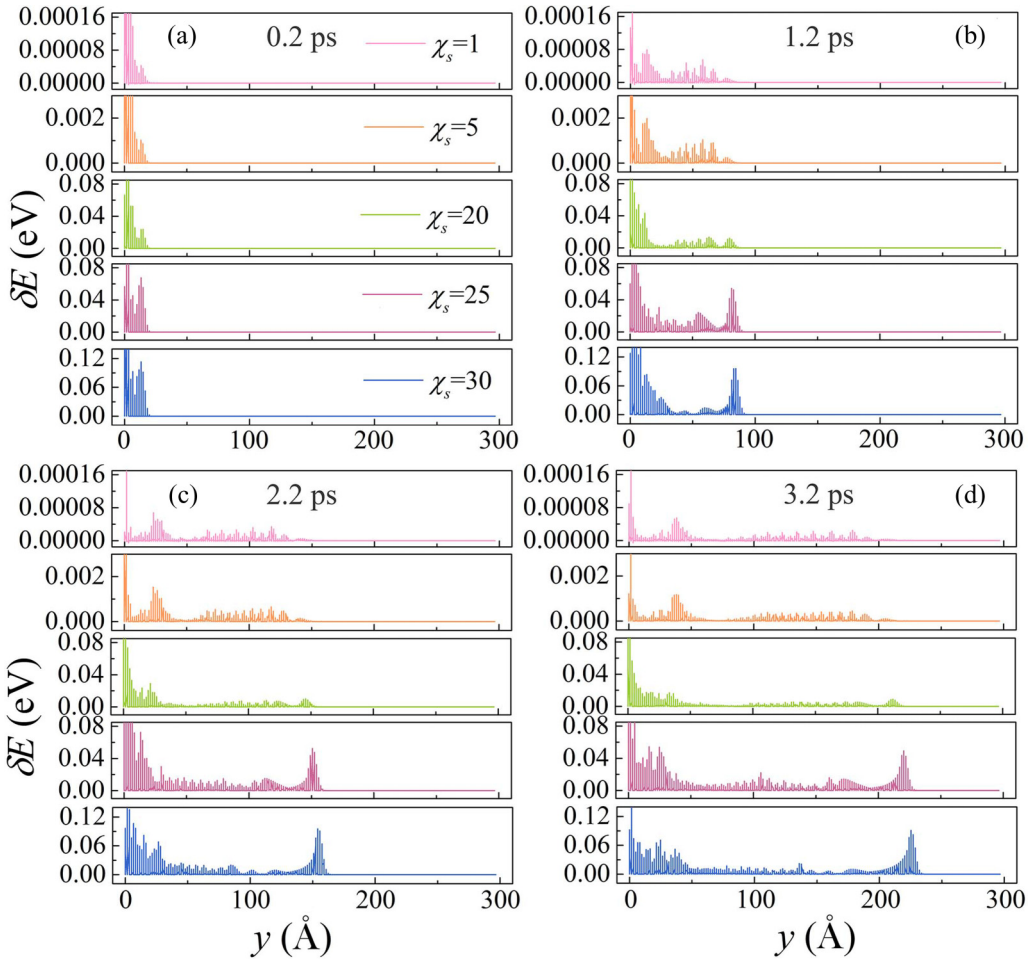

FIG. 2. [(a)–(d)] Time variation of δE under $\chi_S = 1$ and 5 (subsonic thermal excitation), 20, 25, and 30 (supersonic thermal excitation) in the zigzag excitation at simulation times 0.2–3.2 ps. For $\chi_S \leqslant 20$, a series of similar fluctuating wave packets are excited. For $\chi_S \geqslant 25$, a leading shockwave emerges and leaves the fluctuating wave packets far behind.

shockwave passage of a supersonic aircraft reaching further than Mach 1 in the air or the shadowgram of a shockwave from a supersonic bullet in the air, etc. The sonic boom implies that thermal energy in the shockwave would gradually dissipate to the surrounding environment [(later we show that the intensity of shockwave decays exponentially with time in Fig. 3(e)].

The fourth feature is that shockwave intensity is much higher than other fluctuating wave packets and thus it carries a considerable amount of energy in the excitation. To numerically measure the contribution of shockwave to thermal energy transport, we consider the average transport distance of thermal energy d_2 in the zigzag excitation, and d_1 in the armchair excitation (without shockwave generation as an comparison) as [38]

$$d_1 = \frac{\iint (x - x_0)\delta E dx dy}{\iint \delta E dx dy}, \quad d_2 = \frac{\iint (y - y_0)\delta E dx dy}{\iint \delta E dx dy}, \quad (2)$$

where x_0 and y_0 represents the initial excitation position at the sheet edges. Figures 3(a) and 3(b) illustrates the time variation of d_1 and d_2, whose slopes $d'(t)$ provide the numerical measure for the overall thermal transport speed. In the zigzag excitation, for $\chi_S = 5$–20 without shockwave generation, the diffusive-dominated thermal energy transport speed $d_2'(t) = 12.1$–14.6 Å ps. For $\chi_S = 25$–40 with shockwave generation, a sudden jump of the thermal energy transport speed to $d_2'(t) = 27.6$–30.4 Å ps is observed. A shockwave carries a considerable amount of energy away faster than the local acoustic speed. Therefore, shockwave-dominated thermal energy transport exhibits a more than twice efficiency enhancement compared to the diffusive-dominated one. On the other hand, in the armchair excitation, there is no abrupt change in the thermal energy transport speed $d_1'(t) = 6 - 8$ Å/ps since they are all diffusive dominated without shockwave generation. Such anisotropic behavior in the armchair and zigzag directions implies an anisotropic thermal effect of shockwave as an anomalous energy carrier in the BP sheet.

In order to utilize shockwave for possible thermal application, we investigate its kinetic behavior such as intensity, velocity, collision, and strain modulation. Figure 3(c) illustrates the time variation of intensity, I, of five different shockwaves. The intensity I is calculated as the peak value of δE in the shockwave profile. The five different shockwaves are excited by add heat pulse $\chi_S = 25$, 30, 40, 50, and 100, respectively, and a stronger heat pulse corresponds to a higher intensity value. It shows that the shockwaves go through a formation process and then decay with time. For example, for a strong shockwave (initial $I > 0.3$ eV), the intensity rises in the first

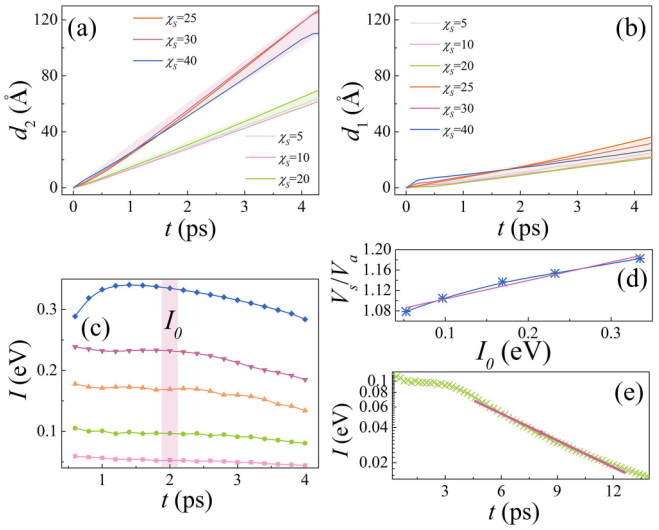

FIG. 3. [(a) and (b)] Average transport distance of thermal energy d_2 (a) in the zigzag excitation and d_1 (b) in the armchair excitation under different excitation strength χ_S. (c) Time variation of shockwave intensity I of 5 shockwaves in 4.0 ps, excited by $\chi_S = 25$, 30, 40, 50, and 100, respectively (from bottom to top). The relative intensity I_0 at 2.0 ps is used to compare the intensity difference. (d) The ratio of shockwave velocity V_s and local acoustic speed V_a, V_s/V_a, as a function of I_0. (e) The logarithm time variation of shockwave intensity I in 14 ps.

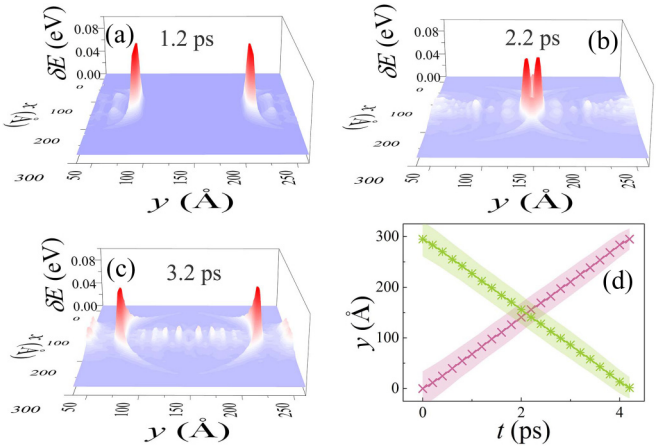

FIG. 4. [(a)–(c)] Snapshots of head-to-head collision between two shockwaves in the BP sheet. (d) Spatial-temporal trajectories of the two shockwaves as a function of y and t. The band indicates their relative intensities.

1.5 ps and then decays afterwards, which implies the absorbing of thermal energy in its formation and the dissipation of thermal energy during propagating.

To investigate the dependence of shockwave velocity on its intensity, we consider the relative intensity, I_0, to numerically measure the intensity difference between different shockwaves. The relative intensity I_0 is measured by the intensity value I at 2.0 ps. As shown in Fig. 3(d), the ratio of shockwave velocity V_s and local acoustic speed V_a, V_s/V_a, monotonically increases with I_0, which is similar to the velocity dependence of solitary waves [24,56,59]. A linear function is used to fit the data as

$$\frac{V_s}{V_a} = k_0 I_0 + 1.067 \tag{3}$$

and the fitted value is $k_0 = 0.36\ \text{eV}^{-1}$. By extending the fitted line to the intercept, it could be derived that the minimum shockwave velocity is no less than $1.067V_a$. Furthermore, to study the decay behavior of I, which numerically clarifies the dissipating process, a long-time simulation of zigzag excitation in a $300\times900\ \text{Å}^2$ BP sheet is performed. As shown in Fig. 3(e), the shockwave intensity I exhibits an approximately exponential decay with time t and is fitted as

$$I \propto \exp(-k_1 t) \tag{4}$$

with the fitted value $k_1 = 0.076\ \text{ps}^{-1}$. It implies that intensity would decay to 20% of the initial value and 80% of energy are dissipated to the surrounding environment in 10 ps. The intensity decay behavior of shockwave separates it from solitary wave whose intensity is time invariant.

To understand the interaction between shockwaves, we investigate the collision of two shockwaves. Figures 4(a)–4(c) illustrates the snapshots of head-to-head collision between two shockwaves from two opposite edges of the BP sheet under $\chi_S = 30$. Unlike solitary waves, the two shockwaves seem exhibit no interaction during the collision process and only leave their tails of sonic boom behind. To numerically identify the noninteractive behavior, the spatial-temporal trajectories of the two shockwaves are plotted in Fig. 4(d). If there were any interactions in the collision process, then a spatial-temporal jump would occur and the trajectory would deviate from its original line, which is known as phase shift [58–61]. Contrary to the behavior of solitary waves, the two shockwaves simply pass through each other without any deviation from their original trajectory lines. It implies that thermal energy carried by shockwaves would maintain its original kinetic properties in the propagation process.

Now we investigate the effect of tensile strain on shockwaves. Tensile strain is the most direct way for manipulating thermal properties that are essentially decided by geometries of atomic structures. Comparing with bulk materials, BP sheet could sustain much larger strain without damaging its structure [45,53,62]. To understand the effect of strain modulation on shockwaves, transverse strain δL_x and longitudinal strain δL_y, are applied along the armchair and zigzag directions, respectively. The strained structure is realized by increasing the simulation box length that corresponds to the lengths of the BP sheet. Here L_x is the armchair length in the x axis and L_y is the zigzag length in the y axis. The atom positions are consistently remapped and the updated length of the BP sheet is $L_x^{'} = L_x(1 + \delta Lx)$ in the armchair direction and $L_y^{'} = L_y(1 + \delta L_y)$ in the zigzag direction. After that, tensile strains are preserved by the fixed condition on the nonexcited edge atoms. Figure 5(a) illustrates the kinetic change of thermal energy transport under subsonic and supersonic thermal excitations. For the phonon response, by applying the longitudinal strain, the wave profile becomes a series of oscillating waves since the stressed phosphorus atoms would vibrate heavily due to the longitudinal excitation. For the shockwave response, by

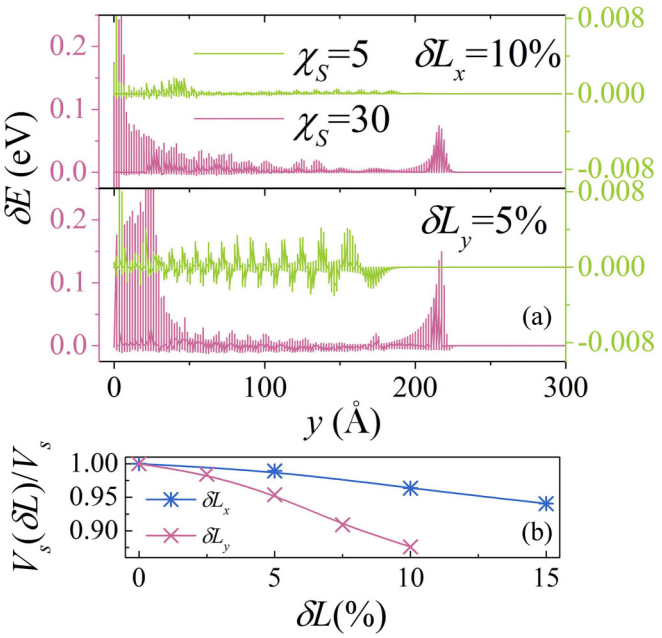

FIG. 5. (a) Thermal energy transport in the zigzag excitation by exerting the transverse strain $\delta L_x = 10$ along the x axis or longitudinal strain $\delta L_y = 5$ along the y axis on the BP sheet. (b) The ratio of shockwave velocity under tensile strain $V_s(\delta L)$ and strain-free velocity V_s, $V_s(\delta L)/V_s$, as a function of transverse strain δL_x and longitudinal strain δL_y.

applying the transverse or longitudinal strain, the shockwave profile remains but its transport velocity decreases with strain. Figure 5(b) illustrates the decrease of shockwave velocity with the strain strength. The decrease tendency is measured by the ratio of shockwave velocity under tensile strain $V_s(\delta L)$ and strain-free velocity V_s, $V_s(\delta L)/V_s$ as

$$\frac{V_s(\delta L_x)}{V_s} \propto -k_2 \delta L_x, \quad \frac{V_s(\delta L_y)}{V_s} \propto -k_3 \delta L_y \tag{5}$$

with the fitted value $k_2 = 0.4$ and $k_3 = 1.5$. It indicates that the longitudinal strain impedes the shockwave transport about 4 times that of the transverse strain. The strain modulation provides a possibility to manipulate the shockwave transport in a continuous range.

IV. CONCLUSION

In summary, we observed that shockwave generates in the zigzag direction of black phosphorene by a strong supersonic thermal excitation above a critical strength. The shockwave exhibits much higher intensity than other fluctuating wave packets and propagates faster than the local acoustic speed with a tail of sonic boom. Consequently, the shockwave-dominated thermal energy transport is twice faster than the diffusive-dominated one. Similarly to solitary waves, shockwave velocity increases linearly with intensity. Contrary to solitary waves, shockwave intensity decays exponentially with time and exhibits the noninteractive collision behavior. Longitudinal and transverse strains are found to be impediment to shockwave propagation. Our finding reveals an anomalous thermal energy transport process in black phosphorene and implies that shockwaves could be utilized for highly efficient thermal transport.

ACKNOWLEDGMENTS

This work was supported by the National Natural Science Foundation of China (Grants No. 11405245, No. 11611240136, No. 21273268, and No. 11574340), Shanghai Natural Science Research Funding (Grant No. 14ZR1448100), the "Hundred People Project" from the Chinese Academy of Sciences, and the Key Research Program of the Chinese Academy of Sciences (Grant No. KJZD-EW-M03). The authors also thank the Knowledge Innovation Program of the Chinese Academy of Sciences, Shanghai Supercomputer Center of China, Computer Network Information Center of Chinese Academy of Sciences, and Special Program for Applied Research on Super Computation of the NSFC-Guangdong Joint Fund (the second phase).

[1] A. Dhar, Adv. Phys. **57**, 457 (2008).
[2] N. Li, J. Ren, L. Wang, G. Zhang, P. Hänggi, and B. Li, Rev. Mod. Phys. **84**, 1045 (2012).
[3] Y. Cai, Q. Ke, G. Zhang, Y. P. Feng, V. B. Shenoy, and Y.-W. Zhang, Adv. Funct. Mater. **25**, 2230 (2015).
[4] R. Fei, A. Faghaninia, R. Soklaski, J.-A. Yan, C. Lo, and L. Yang, Nano Lett. **14**, 6393 (2014).
[5] S. Lee *et al.*, Nat. Commun. **6**, 8573 (2015).
[6] Z. Luo, J. Maassen, Y. Deng, Y. Du, R. P. Garrelts, M. S. Lundstrom, P. D. Ye, and X. Xu, Nat. Commun. **6**, 8572 (2015).
[7] J.-W. Jiang, H. S. Park, and T. Rabczuk, J. Appl. Phys. **114**, 064307 (2013).
[8] J. Hu, X. Ruan, and Y. P. Chen, Nano Lett. **9**, 2730 (2009).
[9] C. Muratore, V. Varshney, J. J. Gengler, J. Hu, J. E. Bultman, A. K. Roy, B. L. Farmer, and A. A. Voevodin, Phys. Chem. Chem. Phys. **16**, 1008 (2014).
[10] J.-W. Jiang, X. Zhuang, and T. Rabczuk, Sci. Rep. **3**, 2209 (2013).
[11] C. Wan *et al.*, Nat. Mater. **14**, 622 (2015).
[12] Z. Liu *et al.*, Nat. Commun. **4**, 2541 (2013).
[13] A. A. Balandin, Nat. Mater. **10**, 569 (2011).
[14] E. S. Reich, Nature **506**, 19 (2014).
[15] D. L. Nika, A. I. Cocemasov, and A. A. Balandin, Appl. Phys. Lett. **105**, 031904 (2014).
[16] A. I. Cocemasov, D. L. Nika, and A. A. Balandin, Nanoscale **7**, 12851 (2015).
[17] J. Chen, Y. Gao, C. Wang, R. Zhang, H. Zhao, and H. Fang, J. Phys. Chem. C **119**, 17362 (2015).
[18] J. Cheh, Y. Gao, C. Wang, H. Zhao, and H. Fang, J. Stat. Mech. (2013) P06009.
[19] J. Chen, C. Wang, N. Wei, R. Wan, and Y. Gao, Nanoscale **8**, 5676 (2016).
[20] W. Qi, J. Chen, J. Yang, X. Lei, B. Song, and H. Fang, J. Phys. Chem. B **117**, 7967 (2013).
[21] C. Wang, L. Zhao, D. Zhang, J. Chen, G. Shi, and H. Fang, J. Phys. Chem. C **118**, 1873 (2014).

[22] N. Li, B. Li, and S. Flach, Phys. Rev. Lett. **105**, 054102 (2010).
[23] H. Zhao, Phys. Rev. Lett. **96**, 140602 (2006).
[24] H. Zhao, Z. Wen, Y. Zhang, and D. Zheng, Phys. Rev. Lett. **94**, 025507 (2005).
[25] S. Lepri, R. Livi, and A. Politi, Phys. Rep. **377**, 1 (2003).
[26] G. Kopidakis, S. Komineas, S. Flach, and S. Aubry, Phys. Rev. Lett. **100**, 084103 (2008).
[27] C. W. Chang, D. Okawa, A. Majumdar, and A. Zettl, Science **314**, 1121 (2006).
[28] J. Cheh and H. Zhao, J. Stat. Mech. (2012) P06011.
[29] M. Alaghemandi, E. Algaer, M. C. Böhm, and F. Müller-Plathe, Nanotechnology **20**, 115704 (2009)
[30] E. Gonzalez Noya, D. Srivastava, and M. Menon, Phys. Rev. B **79**, 115432 (2009).
[31] C. W. Chang, D. Okawa, H. Garcia, A. Majumdar, and A. Zettl, Phys. Rev. Lett. **101**, 075903 (2008).
[32] X. Xu *et al.*, Nat. Commun. **5**, 3689 (2014).
[33] P. Cipriani, S. Denisov, and A. Politi, Phys. Rev. Lett. **94**, 244301 (2005).
[34] E. Arévalo, F. G. Mertens, Y. Gaididei, and A. R. Bishop, Phys. Rev. E **67**, 016610 (2003).
[35] S. Chen, Y. Zhang, J. Wang, and H. Zhao, Phys. Rev. E **87**, 032153 (2013).
[36] J. Yang, Y. Zhang, J. Wang, and H. Zhao, Phys. Rev. E **83**, 052104 (2011).
[37] S. Chen, Y. Zhang, J. Wang, and H. Zhao, Science China-Phys. Mech. Astron. **56**, 1466 (2013).
[38] J. Chen, S. Chen, and Y. Gao, J. Phys. Chem. Lett. **7**, 2518 (2016).
[39] L. Chen and S. Kumar, J. Appl. Phys. **110**, 074305 (2011).
[40] T. Kim, M. A. Osman, C. D. Richards, D. F. Bahr, and R. F. Richard, Phys. Rev. B **76**, 155424 (2007).
[41] J. Chen, W. Qi, M. Zhang, and H. Zhao, J. Stat. Mech. (2015) P06007.
[42] J. Cheh and H. Zhao, J. Stat. Mech. (2011) P10031.
[43] A. Jain and A. J. H. McGaughey, Sci. Rep. **5**, 8501 (2015).
[44] M. Engel, M. Steiner, and P. Avouris, Nano Lett. **14**, 6414 (2014).
[45] R. Fei and L. Yang, Nano Lett. **14**, 2884 (2014).
[46] J.-W. Jiang and H. S. Park, Nat. Commun. **5**, 4727 (2014).
[47] X. Wang *et al.*, Nat. Nanotech. **10**, 517 (2015).
[48] J. Guan, Z. Zhu, and D. Tománek, Phys. Rev. Lett. **113**, 046804 (2014).
[49] See Supplemental Material at http://link.aps.org/supplemental/10.1103/PhysRevB.95.134301 for PS1. Anisotropic Sound Velocity of Black Phosphorene, and PS2. Shockwave in BP Sheet with Large Lateral Size, and PS3. Shockwave in BP Sheet with Modified Energy Parameters.
[50] Y. Hong, J. Zhang, X. Huang, and X. C. Zeng, Nanoscale **7**, 18716 (2015).
[51] J.-W. Jiang, T. Rabczuk, and H. S. Park, Nanoscale **7**, 6059 (2015).
[52] Y.-Y. Zhang, Q.-X. Pei, J.-W. Jiang, N. Wei, and Y.-W. Zhang, Nanoscale **8**, 483 (2016).
[53] Z.-D. Sha, Q.-X. Pei, Z. Ding, J.-W. Jiang, and Y.-W. Zhang, J. Phys. D: Appl. Phys. **48**, 395303 (2015).
[54] S. Plimpton, J. Comput. Phys **117**, 1 (1995).
[55] J. D. J. Anderson, *Fundamentals of Aerodynamics*, 3rd ed. (McGraw-Hill, New York, 2001).
[56] P. G. Drazin and R. S. Johnson, *Solitons: An Introduction*, 2nd ed. (Cambridge University Press, Cambridge, 1989).
[57] S. Tang, F. Tesler, F. G. Marlasca, P. Levy, V. Dobrosavljević, and M. Rozenberg, Phys. Rev. X **6**, 011028 (2016).
[58] L. R. Veeser and J. C. Solem, Phys. Rev. Lett. **40**, 1391 (1978).
[59] T. Y. Astakhova, M. Menon, and G. A. Vinogradov, Phys. Rev. B **70**, 125409 (2004).
[60] T. Jin, H. Zhao, and B. Hu, Phys. Rev. E **81**, 037601 (2010).
[61] H. Ikezi, R. J. Taylor, and D. R. Baker, Phys. Rev. Lett. **25**, 11 (1970).
[62] Z.-Y. Ong, Y. Cai, G. Zhang, and Y.-W. Zhang, J. Phys. Chem. C **118**, 25272 (2014).